Supplementary information (SI)

The relationship between pore architecture of MFI zeolite and isoamylene oligomerization

Zijian Wang[a], Jiashuo Zheng[b], Jiahan Li[c], Hao Pang[a], Ming Ke[c], Zhaozheng Song[c]*

(a. Institute of Chemical Engineering, Guangdong Academy of Sciences, Guangdong, China; b. College of Chemistry, Nankai University, Tianjin, China; c. College of Science, China University of Petroleum, Beijing, China)

1 Analysis of synthesis

Silicalite-1 zeolite is used as the crystal seed. XRD pattern (Fig. S1) shows that the crystal is the typical MFI zeolite. And the SEM image (Fig. S2) indicates that the crystal exhibits flake-like morphology with a width and thickness of approximately 220 nm and 120 nm, respectively.

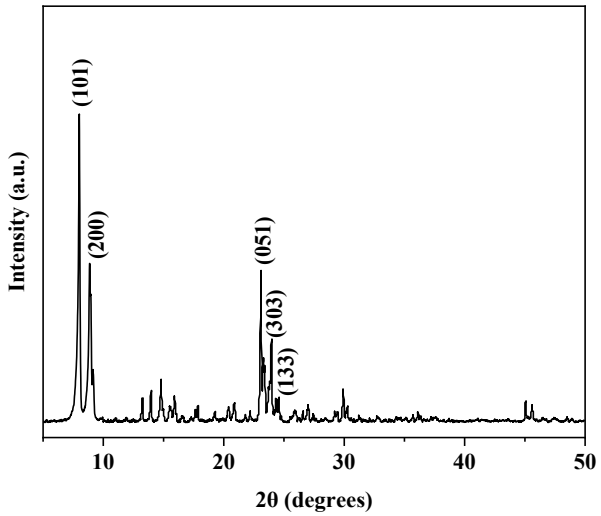

Fig. S1 XRD pattern of Silicalite-1 zeolite

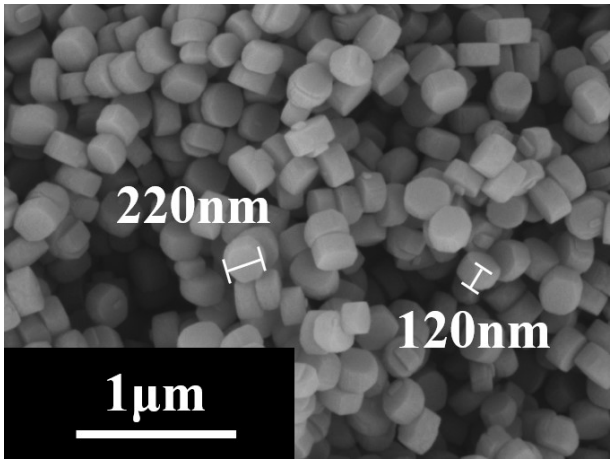

Fig. S2 SEM image of Silicalite-1 zeolite

2 Analysis of catalytic performance

2.1 Qualitative and quantitative methods

The Agilent 7890A gas chromatograph with FID detector and HP-5 column (60 m, 0.25×0.25 μ m) was used to analyze the liquid phase products. The initial temperature of the column box was 303 K, and it was heated to 523 K at a rate of 8 K/min and maintained for 0 min. The feed rate was 0.2 μl and the split ratio was 180:1. Under these conditions, the correction factors for 2-methyl-2-butene, 1-decene, and 1-pentadecene were adjusted to obtain more accurate contents by utilizing n-heptane as the internal standard. The Fig. S3 shows that three components with different contents have a good linear response relationship with n-heptane. The correction factors for 2-methyl-2-butene, 1-decene, and 1-pentadecene were 1.043, 0.988, and 0.992 respectively.

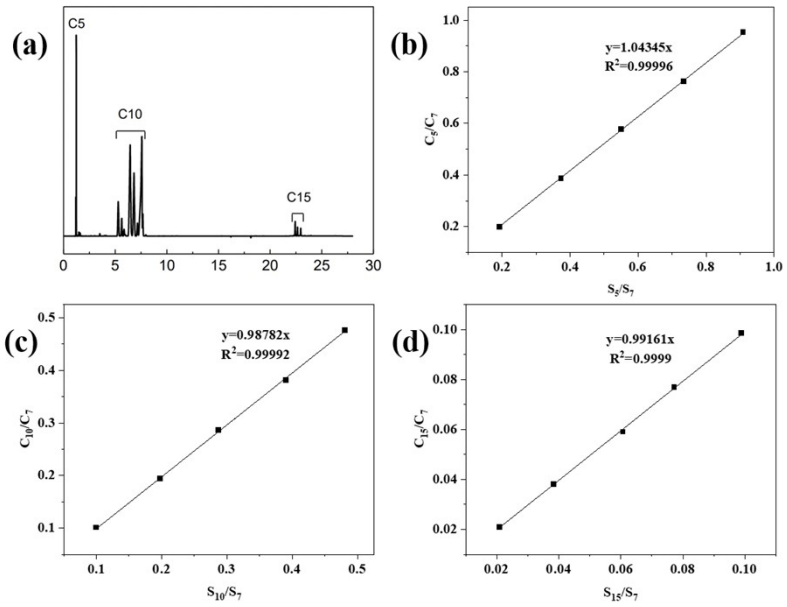

Fig. S3 Typical chromatogram of C_5 oligomeric products (a) and calibration curves

(b. C_5; c.C_{10}; d. C_{15})

2.2 Analysis of dimerization product selectivity

The dimerization product selectivity of MFI samples at different time is shown in Tab. S1. The catalytic characteristics of different samples are relatively stable within 12 h. In general, the dimerization product selectivity of MFI-28(Br) and MFI-84(Br) is higher than that of MFI-21(Br) and MFI-56(Br) with similar morphologies, respectively. And the dimerization product selectivity of MFI-21(Br) and MFI-28(Br) is higher than that of MFI-56(Br) and MFI-84(Br) due to their better microporous selectivity. Although MFI-28(OH) rapidly deactivates within 12 h, its more complete microporous structure results in the highest selectivity for dimerization products.

Tab. S1 Dimerization product selectivity of MFI samples

Sample	2h	4h	6h	8h	10h	12h
MFI-21(Br)	82.92	78.91	82.33	82.68	83.57	80.22
MFI-28(Br)	90.72	87.66	86.19	85.49	88.76	85.05
MFI-56(Br)	78.58	78.15	79.63	80.39	81.79	79.85
MFI-84(Br)	83.95	81.06	80.03	82.58	81.35	85.06
MFI-28(Br)-TP	54.90	52.04	50.63	53.85	52.56	53.63
MFI-28(OH)	92.76	87.78	83.71	86.85	82.88	86.05
MFI-28(OH)-TP	64.05	66.01	67.58	73.70	69.01	67.19

2.3 Analysis of molecular dynamics

The MFI model is downloaded from the IZA structure database [1]. During the MD simulation process, the 2 × 2 × 2 supercells are selected. The diffusion process of guest molecules in zeolite is carried out under infinite dilution conditions (4 molecules per each supercell). The simulations are performed in the canonical ensemble (NVT) [2], in which the number of particles (N), simulated volume (V) and temperature (T) are kept constant. In addition, the simulated temperature in our study is maintained at 423 K and is controlled by a Nose-Hoover thermostat, which is consistent with the actual temperature. The velocity Witt algorithm is used to integrate the Newtonian equation of motion. The long-range electrostatic interaction is calculated with the Ewald summation method and the Lennard-Jones interaction of the cut-off radius is 18.5 Å. This work uses a Dreiding force field widely used in studying the zeolites [3,4]. And the optimized structure of different complexes are as shown in Fig. S4.

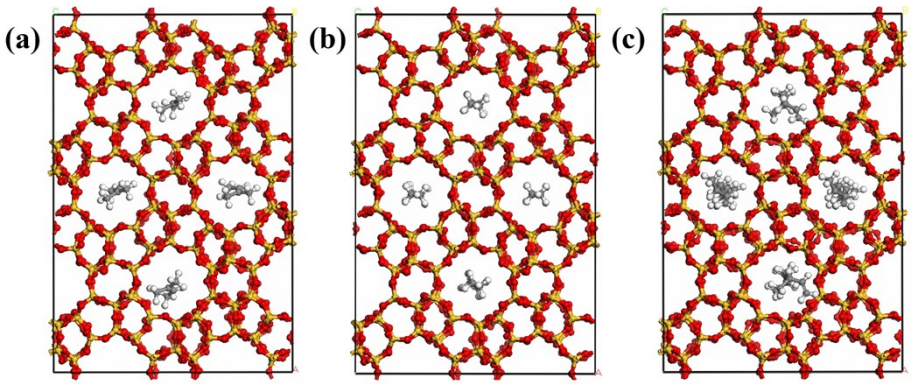

Fig. S4 Optimized structure of different complexes (a) i-C_5, (b) n-C_7, (c) i-C_{10}

To be specific, the optimized structure is subjected to annealing simulation to obtain at least 5

sets of annealing configurations. During MD simulation, the simulation timestep is 1 fs. Among them, the molecules of isoamylene, n-heptane and isodecene run for 1×10^7 steps. The trajectory is recorded every 1000 steps. And the mean square displacement (MSD) is analyzed, which is an important parameter to characterize the diffusion behavior. MSD of an adsorbed molecule is defined as the following formula (Eq.(1)), where N_m is the number of adsorbed molecules, N_τ is the number of time origins used in calculating the average, and r_i is the coordinate of the center of mass of molecule i. What's more, the slope of the MSD as a function of time determines the self-diffusion coefficient (D_s), defined for the three-dimensional diffusion according to the so-called Einstein relation (Eq.(2)), where b is the thermal factor arising from atomic vibrations.

$$MSD = \frac{1}{N_m}\sum_{i}^{N_m}\frac{1}{N_\tau}\sum_{t_0}^{N_t}[r_i(t_0+\tau)-r_i(t_0)]^2 \qquad (1)$$

$$MSD = 6D_S\tau + b \qquad (2)$$

Next, the self-diffusion coefficients of three molecules are obtained according to the MSD fitting curves (Fig. S5). It is shown that the self-diffusion coefficient of n-heptane is significantly higher than that of 2-methyl-2-butene and decene under the low temperature condition. On the one hand, the carbon-carbon double bond and steric hindrance are not conducive to the diffusion of branched alkanes in zeolite [5]. On the other hand, low temperature is beneficial to reduce the thermal resistance effect of linear alkanes [6].

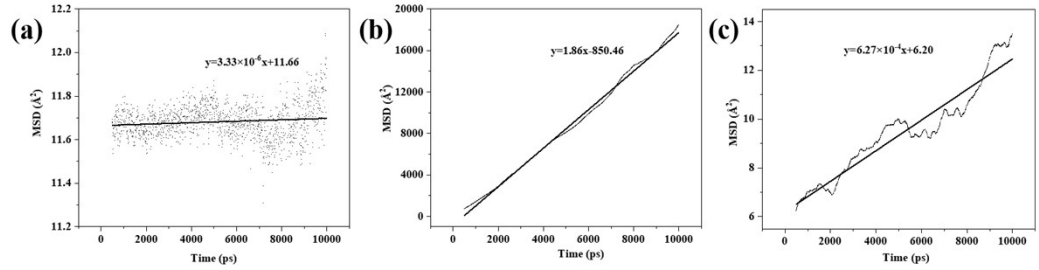

Fig. S5 MSD fitting curves of isoamylene (a), n-heptane (b) and isodecene (c) in MFI zeolites

3 Analysis of growth mechanism

3.1 Component analysis

Organic structure directing agents (OSDAs) not only have the effects on template and structure-directing, but also can fill the channels of zeolite. Iorio et al. [7] believed the $TMAda^+$ and alkaline cation balanced the negative charges in synthetic zeolites. In this work, TPA can be estimated by calculating the decrease in weight between 433 K and 923 K under air atmosphere [8]. Fig. S6 shows

the weight loss curves of different as-synthesized MFI samples. The weight loss percentages of the samples are 8.58 %, 8.59 %, 10.44 % and 10.16 % respectively, which indicate that the ratio of TPA/Al grows as the SiO_2/Al_2O_3 ratio increases. According to DTG analysis, the peaks of MFI-56 (Br) and MFI-84(Br) shift towards higher temperatures compared with MFI-21(Br) and MFI-28(Br), which may be attributed to the different morphologies and the content of organic amines.

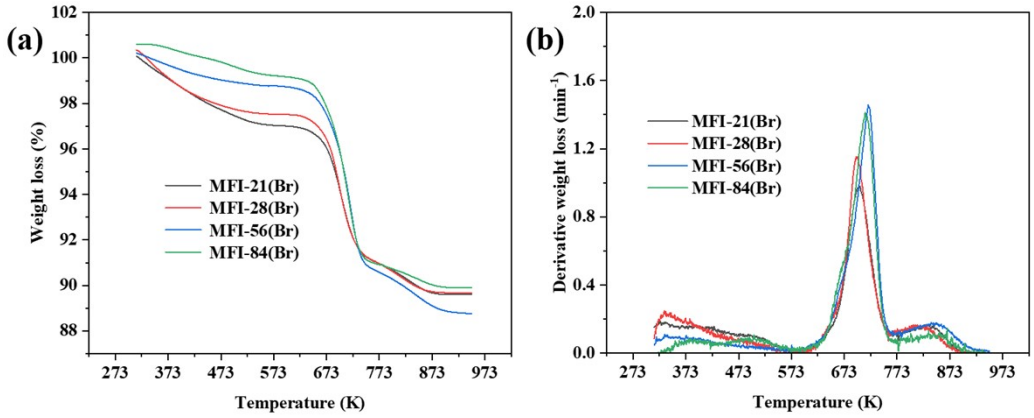

Fig. S6 TG (a) and DTG (b) plot of as-synthesized MFI samples

The compositions of MFI samples with different SiO_2/Al_2O_3 ratios synthesized are analyzed in the Tab. S2. Si, Al, while Na elements are analyzed by ICP-OES instrument. And TPA are calculated mentioned above (Fig. S6).

Tab. S2 Composition analysis of MFI samples (mol)

(a.ICP-OES Analysis;b. TG Analysis)

Sample	SiO_2/Al_2O_3[a]	Na/Al[a]	HMI/Al[b]
MFI-21(Br)	21.56	0.78	0.38
MFI-28(Br)	25.52	0.70	0.51
MFI-56(Br)	32.63	0.46	0.66
MFI-84(Br)	55.65	0.76	1.19

3.2 Simulation calculation

The single unit cell model (Fig. S7) utilizing periodic density functional theory is optimized without violating the Löwenstein' rule. The generalized gradient approximation (GGA) and perdew-Burke-Emzerhof (PBE) exchange correlation function were used, and the TS method was utilized for DFT-D correction [9], with the D-polarization function augmented double numerical atomic orbitals (DNP) as the basis set [10]. And the Monkhost-Pack grid with a k-point meshes of 1×1×1 was applied. GC-MC simulation is employed to predict the potential positioning of Na^+ in the

optimization framework of different SiO_2/Al_2O_3 ratios. The adsorption simulation uses Mulliken charges calculated by periodic density functional theory, selecting the Dreiding force field [3,4] with ultra-fine calculation accuracy. The adsorption simulation results are shown in Fig. S8, which indicate that Na^+ can be found in both the sinusoidal channels and the straight channels.

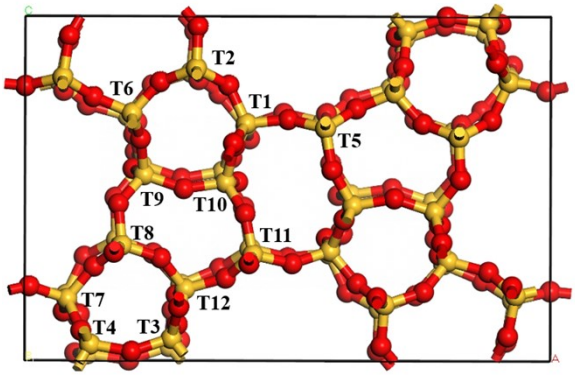

Fig. S7 Location of different T sites in MFI zeolite

(Si: yellow; O: red)

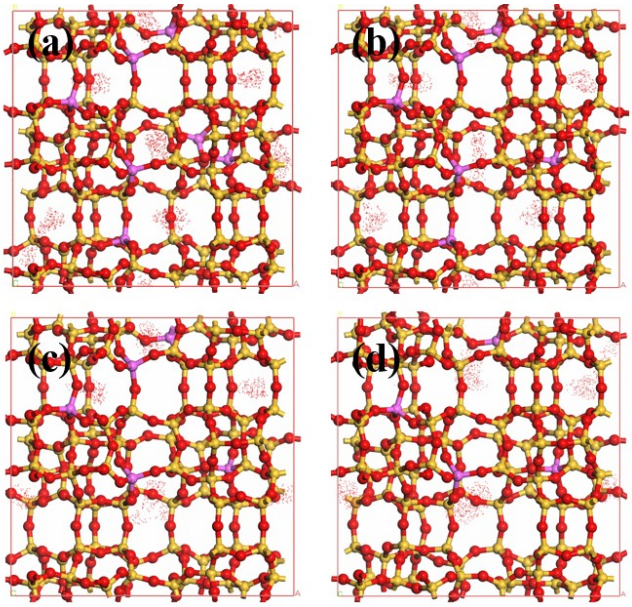

Fig. S8 GC-MC simulations of samples with different SiO_2/Al_2O_3 ratios

(Si: yellow; O: red; Al: purple)

Na^+ and TPA^+ are placed in the intersection and the location near aluminum respectively as the initial structure to analyze theirs effects on the position of Al in the framework. And the optimized structures are shown in Fig. S9 and Fig. S10.

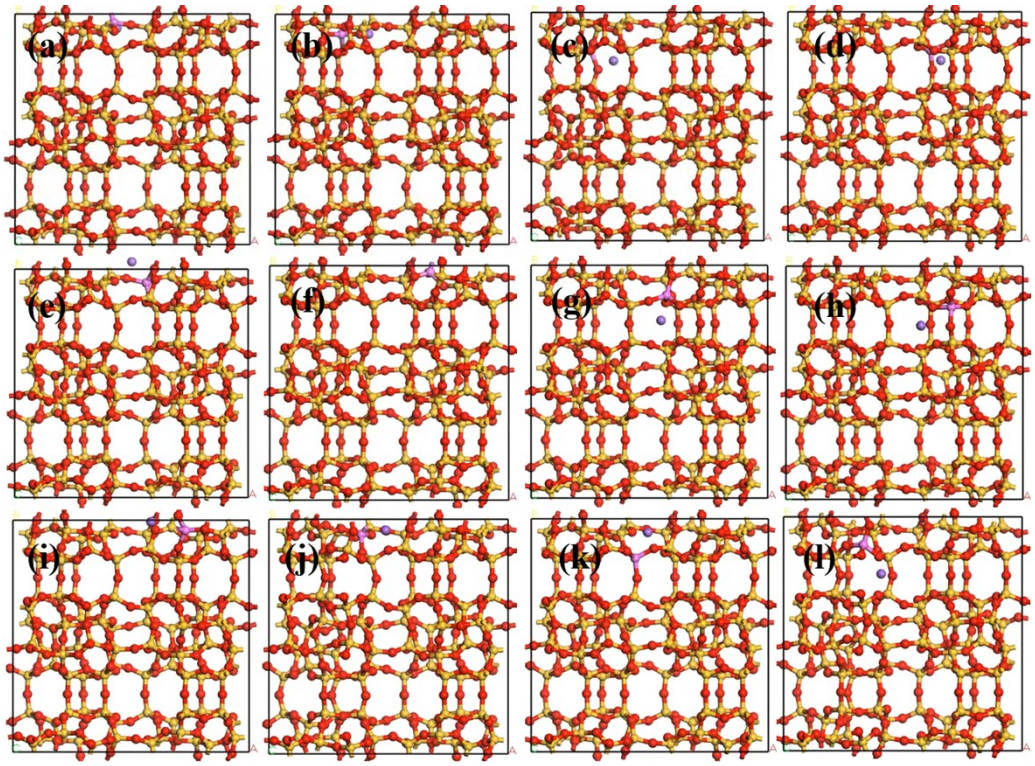

Fig. S9 Optimized structure of Na-MFI at different T sites

(Si: yellow; O: red; Al: pink; Na^+: purple)

Tab. S3 Na-MFI complexes with Al substitute at different Al positions

	E_{sub} (kJ/mol)	MFI framework (e)	Na^+ (e)	r(Na-Al) (Å)
T_1	29.00	-0.811	0.811	3.124
T_2	45.33	-0.782	0.782	2.940
T_3	67.44	-0.815	0.815	3.019
T_4	25.90	-0.800	0.800	3.027
T_5	23.29	-0.791	0.791	3.065
T_6	50.38	-0.836	0.836	3.066
T_7	40.61	-0.772	0.772	3.132
T_8	54.92	-0.737	0.737	3.079
T_9	25.80	-0.796	0.796	3.017
T_{10}	24.40	-0.793	0.793	4.692
T_{11}	9.06	-0.792	0.792	3.174
T_{12}	0	-0.770	0.770	3.078

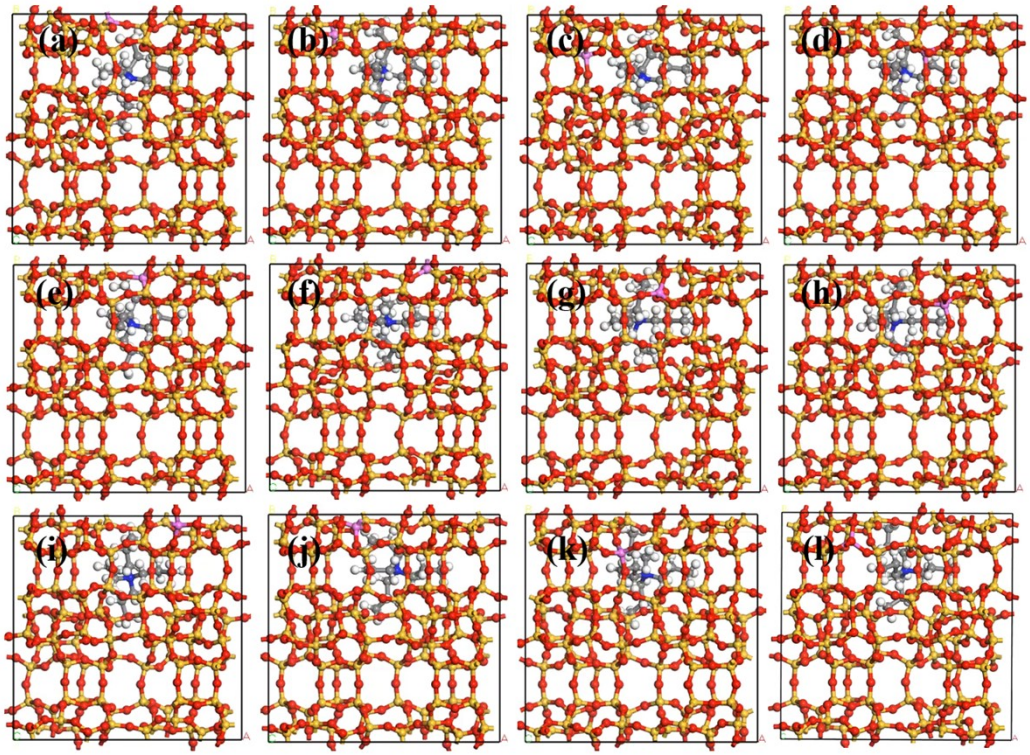

Fig. S10 Optimized structure of TPA-MFI at different T sites

(Si: yellow; O: red; Al: pink; N: blue; C: grey; H: white)

Tab. S4 TPA-MFI complexes with Al substitute at different Al positions

	E_{sub} (kJ/mol)	MFI framework (e)	$-N^+-$ (e)	r(N-Al) (Å)
T_1	40.06	-0.924	-0.376	6.131
T_2	52.73	-0.941	-0.381	5.918
T_3	26.72	-0.930	-0.378	5.291
T_4	16.12	-0.935	-0.386	5.648
T_5	35.76	-0.926	-0.378	5.133
T_6	5.08	-0.933	-0.384	5.716
T_7	13.97	-0.939	-0.367	7.667
T_8	50.33	-0.940	-0.371	9.874
T_9	0	-0.936	-0.378	12.675
T_{10}	60.83	-0.955	-0.369	8.147
T_{11}	45.34	-0.926	-0.378	8.137
T_{12}	27.60	-0.945	-0.377	11.883

3.3 ssNMR Analysis

^{27}Al MAS NMR and 2D ^{27}Al MQ MAS NMR experiments are performed at 18.8 T magnetic field on spectrometers by Avance neo 600 instrument. The tests are conducted by utilizing as-calcined samples. Specifically, ^{27}Al MAS NMR at 25 kHz is carried out with 512 sample cycles accompanied by an acquisition time of 0.0434 s and a delay time of 2 s (Larmor frequency of 156.4 MHz for ^{27}Al). 2D ^{27}Al MQ MAS NMR experiments are performed at a size of fid of 80 in F_1 and 512 in F_2, and the number of scans is 256. Sampling times of 0.005 s for F_1 and 0.05 s for F_2 are accompanied by a Dwell time of 10.6 μs and a Pre-scan delay of 6.50 μs. ^{27}Al MQ MAS and ^{27}Al are acquired at 25K Hz on a 2.5 mm H/X MAS Bruker probe. ^{27}Al and ^{27}Al 3Q MAS use 0.1 M solution of Al $(NO_3)_3$ at 0 ppm as a reference. According to the F_1 dimension information, the chemical shifts of different framework aluminum species in the F_2 dimension are identified as $T_{(a)}$, $T_{(b)}$, $T_{(c)}$, $T_{(d)}$ and $T_{(e)}$ respectively (Fig. S11) [11].

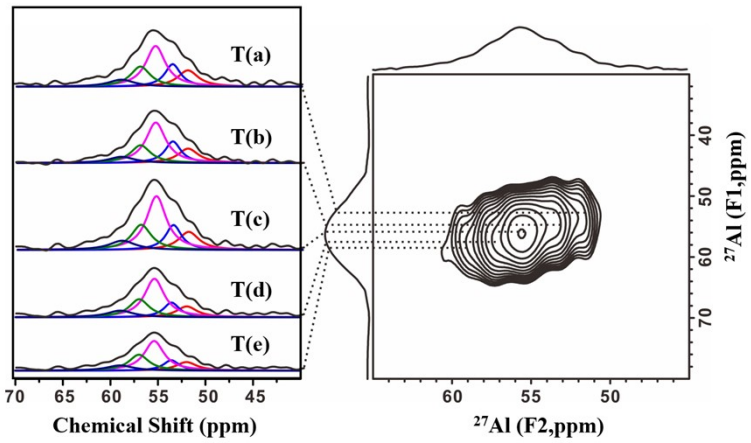

Fig. S11 2D ^{27}Al MQ MAS NMR spectrum of MFI-28(Br) sample at 18.8 T

Tab. S5 Detailed simulation parameters obtained from the sliced spectra of MQ MAS spectra

T site	$F1_{ppm}$	$F2_{ppm}$	PQ_{MHz}	σ_{iso}
$T_{(a)}$	53.1	52.0	1.62	52.7
$T_{(b)}$	54.0	53.6	0.98	53.9
$T_{(c)}$	56.1	55.4	1.29	55.8
$T_{(d)}$	57.9	57.0	1.47	57.6
$T_{(e)}$	59.8	59.0	1.38	59.5

[a] Chemical shift along F_1 dimension in ppm

[b] Chemical shift along F_2 dimension in ppm

[c] Isotropic chemical shift values obtained by fitting each sliced spectrum

[d] $PQ = CQ(1+\eta^{2/3})^{1/2}$

PQ : Quadrupolar product parameter

The ^{27}Al MAS NMR spectra and fitting peak results of different samples are shown in the Fig. S12 and Tab. S6. MFI-21(Br) skeleton aluminum is more focused on $T_{(e)}$ site, and gradually decreases as the ratio of SiO_2/Al_2O_3 increases. Finally, it is more concentrated at the $T_{(b)}$ site. There is no significant correlation between the relative content of $T_{(a)}$, $T_{(c)}$, and $T_{(d)}$ sites and the ratio of SiO_2/Al_2O_3. However, compared with MFI-56(Na) and MFI-84(Na) synthesized without TPA, a significant increase in $T_{(c)}$ site can be observed.

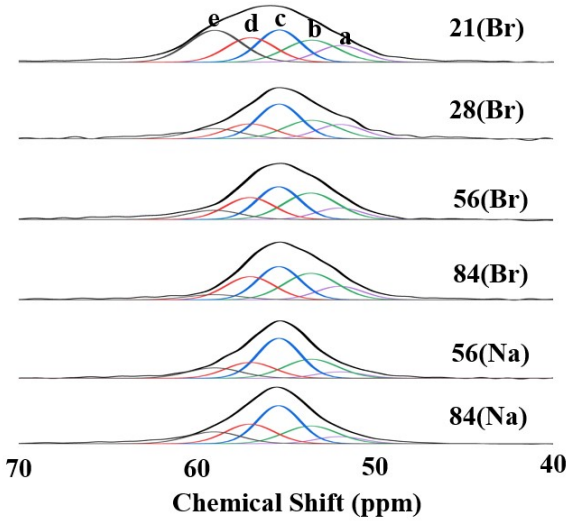

Fig. S12 ^{27}Al MAS NMR spectra of MFI samples

Tab. S6 T-site fitting peaks of MFI samples

Sample	$T_{(a)}$ (%)	$T_{(b)}$ (%)	$T_{(c)}$ (%)	$T_{(d)}$ (%)	$T_{(e)}$ (%)
MFI-21(Br)	12.56	18.87	22.09	19.19	27.28
MFI-28(Br)	15.22	22.37	33.62	16.44	12.34
MFI-56(Br)	10.96	28.77	28.50	21.84	9.93
MFI-84(Br)	12.98	29.04	29.16	23.21	5.61
MFI-56(Na)	6.89	23.36	39.28	17.73	12.74
MFI-84(Na)	7.34	21.06	36.29	21.27	14.04

References

[1] https://www.iza-online.org/

[2] S. Hashemi, *Physica Scripta*, 95(2020) 075701.

[3] K. Muraoka, W. Chaikittisilp, Y. Yanaba, T. Yoshikawa, T. Okubo, *Angewandte Chemie International Edition*, 57 (2018) 3742-3746.

[4] J. E. Schmidt, D. Fu, M. W. Deem, B. M. Keckhuysen, *Angewandte Chemie International Edition*, 55 (2016) 16044-16048.

[5] D. Schhuring, A. P. J. Jansen, R. A. Santen, *The Journal of Physical Chemistry B*, 104(2000) 941-948.

[6] J. Yuan, Z. Liu, Y. Wu, J. Han, X. Tang, C. Li, W. Chen, X. Yi, J. Zhou, R. Krishna, G. Sastre, A. Zheng, *Proceedings of the National Academy of Sciences of the United States of America*, 118(2021) e2102097118.

[7] J. R. D. Iorio, S. Li, C. B. Jones, C. T. Nimlos, Y. Wang, E. Kunkes, V. Vattipalli, S. Prasad, A. Moini, W. F. Schneider, R. Gounder, *The Journal of American Chemical Society*, 142(2020), 4807-4819.

[8] P. Wu, Q. B. Kan, N. Xu, D. Y. Wang, Y. C. Shang, M. P. Su, T. H. Wu, *Acta Chimica Sinica*, 61(2003), 1202-1207.

[9] J. P. Perdew, K. Burke, M. Ernzerhof, *Physical Review Letters*, 77(1997) 3865-3868.

[10] B. Delle, *The Journal of Chemical Physics*, 92(1990) 508-517.

[11] T. Yokoi, H. Mochizuki, S. Namba, J. N. Kondo, T. Tatsumi, *The Journal of Physical Chemistry*, 119(2015) 15303-15315.